High-Pitch Formant Estimation by Exploiting Temporal Change of Pitch

High-Pitch Formant Estimation by Exploiting Temporal Change of Pitch

Tianyu T. Wang, *Student Member, IEEE*, and Thomas F. Quatieri, *Fellow, IEEE*

***Abstract*—This paper considers the problem of obtaining an accurate spectral representation of speech formant structure when the voicing source exhibits a high fundamental frequency. Our work is inspired by auditory perception and physiological studies implicating the use of pitch dynamics in speech by humans. We develop and assess signal processing schemes aimed at exploiting temporal change of pitch to address the high-pitch formant frequency estimation problem. Specifically, we propose a 2-D analysis framework using 2-D transformations of the time–frequency space. In one approach, we project changing spectral harmonics over time to a 1-D function of frequency. In a second approach, we draw upon previous work of Quatieri and Ezzat *et al.* [1], [2], with similarities to the auditory modeling efforts of Chi *et al.* [3], where localized 2-D Fourier transforms of the time–frequency space provide improved source-filter separation when pitch is changing. Our methods show quantitative improvements for synthesized vowels with stationary formant structure in comparison to traditional and homomorphic linear prediction. We also demonstrate the feasibility of applying our methods on stationary vowel regions of natural speech spoken by high-pitch females of the TIMIT corpus. Finally, we show improvements afforded by the proposed analysis framework in formant tracking on examples of stationary and time-varying formant structure.**

***Index Terms*—Formant estimation, high-pitch effects, linear prediction, spectrotemporal analysis, temporal change of pitch.**

I. Introduction

ESTIMATING the formant frequencies of a speaker during vowel utterances is a fundamental problem of speech analysis. Current state-of-the-art formant estimation systems typically perform short-time analysis in conjunction with a tracking mechanism (Fig. 1). For example, in [4], short-time analysis is used to generate linear predictive cepstral coefficients (LPCC) which are used as observations in a Kalman filtering framework. This paper focuses on the analysis component (shaded, Fig. 1) of such systems in relation to formant estimation of high-pitch speakers (e.g., with pitch values ranging from 150 to 450 Hz). Under such conditions, short-time traditional and homomorphic linear prediction analysis (by which LPCC are obtained) are known to provide inadequate representations of the formant structure [5], [6]. This paper addresses this limitation in analysis by exploiting temporal changes in pitch.

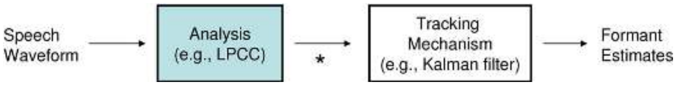

Fig. 1. Schematic illustrating typical formant estimation system with analysis stage (shaded) and tracking mechanism. Estimates can also be obtained *directly* from the output of the analysis component (*) without the tracking mechanism.

The current work is inspired by psychophysical and physiological studies of the auditory system implicating its use of pitch dynamics in processing speech. For instance, McAdams showed in a series of concurrent vowel segregation tasks that subjects reported an increased "prominence" percept for vowels whose pitch was modulated relative to those that were not modulated [7]. In another study by Diehl *et al.* [8], although limited to a two-category vowel identification task, results indicated that a linearly changing pitch can improve human vowel identification accuracy. In both studies, the observed effects were greatest when the synthetic source was chosen to have a high pitch (e.g., $\sim$250–400 Hz). Physiological models of the auditory system (e.g., [3]) have also proposed that high-level cortical processing analyzes an auditory-based time–frequency distribution in both the temporal and spectral dimensions, thereby exploiting temporal changes in speech such as pitch dynamics.

The auditory model proposed by Chi *et al.* [3] may be viewed as one realization of a generalized two-dimensional (2-D) processing framework. In our work, we develop and assess realizations of this framework for improving high-pitch formant estimation. The foundation for our framework was first introduced in [9], [10]. In one approach, we project changing pitch harmonics to a single function of frequency to improve the spectral sampling of a stationary formant envelope under high-pitch conditions. This initial step is similar to the multiframe analysis method proposed by Shiga and King [11], in which iterative techniques were subsequently used to derive a cepstrum best fit to the collection of harmonic peaks in a least-squared-error sense. Alternatively, in this paper, we perform a simple interpolation across the harmonic peaks to generate a magnitude spectrum to be used with the autocorrelation method of linear prediction. In the second approach, we compute two-dimensional Fourier transforms of spectrotemporally local regions of the short-time Fourier transform magnitude as proposed by Quatieri [1] and extended by Ezzat

Manuscript received July 25, 2008; revised May 08, 2009. First published June 05, 2009; current version published October 23, 2009. This work was supported by the Department of Defense under Air Force Contract FA8721 05 C 0002. The work of T. T. Wang was additionally supported by the National Institutes of Deafness and Other Communicative Disorders under Grant 5 T 32 DC00038. The opinions, interpretations, conclusions, and recommendations are those of the authors and are not necessarily endorsed by the United States Government. The associate editor coordinating the review of this manuscript and approving it for publication was Dr. Malcolm Slaney.

The authors are with the Lincoln Laboratory, Massachusetts Institute of Technology, Lexington, MA 02173 USA, and also with the Program in Speech and Hearing Bioscience and Technology, Harvard–MIT Division of Health Sciences and Technology, Cambridge, MA 02139 USA (e-mail: ttwang@ll.mit.edu; quatieri@ll.mit.edu).

Color versions of one or more of the figures in this paper are available online at http://ieeexplore.ieee.org.

Digital Object Identifier 10.1109/TASL.2009.2024732

et al. [2]. Ezzat *et al.* have made phenomenological observations regarding the source-filter separability of this transformed space. In our paper, we argue for these observations analytically and exploit this characteristic to improve high-pitch formant estimation.

We emphasize that this work focuses on improving the analysis framework used in formant estimation for high-pitch vowels rather than performing formant tracking (e.g., in conjunction with Kalman filtering [4]). We therefore obtain formant estimates directly from the output of the analysis framework (*, Fig. 1) through linear prediction analysis rather than through a tracking mechanism. Furthermore, our evaluation primarily focuses on the canonical problem of estimating formant frequencies under the assumption of a stationary vocal tract (i.e., monophthong vowels) but with the added constraint that pitch is changing throughout the duration of the stationary vowel. These conditions will be shown to be often present on natural vowels extracted from the standard TIMIT corpus [12]. The constraint of changing pitch will also be argued to be a modest one with regards to the degree of pitch change required to obtain improvements in formant estimates. Finally, we will demonstrate that the proposed 2-D framework can provide improvements in formant tracking for both the stationary and time-varying vocal tract conditions. As will be subsequently discussed, these improvements can be obtained whenever the pitch dynamics and formant trajectories of a vowel are moving in distinct directions. This more generalized set of conditions for improving formant estimates may be explored in future work towards a full formant-estimation system that incorporates a tracking mechanism.

This paper is organized as follows. Section II briefly reviews the problem of high-pitch formant estimation using a frequency-domain view often referred to as spectral undersampling. We propose a 2-D analysis framework in contrast to traditional short-time analysis for addressing this issue under certain conditions. Section III describes specific formant estimation methods motivated from our observations in Section II. Section IV presents a comparative evaluation of formant frequency estimates from these methods using synthetic vowels. In Section V, to demonstrate the feasibility of our analysis methods on natural speech, we present formant estimation results on monophthong vowels spoken by high-pitch females from the TIMIT corpus. In Section VI, we demonstrate the implications of our work for formant tracking of monophthong vowels, comparing standard LPCC analysis with the proposed 2-D framework in several tracking tasks. Section VII extends these efforts by demonstrating the feasibility of applying the proposed 2-D framework to formant tracking of a time-varying vocal tract configuration. Section VIII summarizes our conclusions and describes future directions.

II. Two-Dimensional Processing Framework

A long-standing problem in formant estimation is that of obtaining accurate estimates for high-pitch speakers. Existing analysis methods are known to provide poor representations of the formant structure for a high-pitch source signal. For instance, traditional linear prediction suffers from aliased autocorrelation coefficients while cepstral analysis on high-pitch speech results in reduced source-filter separability in the quefrency domain [5]. In this paper, we adopt an equivalent view of this difficulty in analysis referred to as spectral *undersampling*. Specifically, from the traditional source-filter production model for vowels, a periodic source signal can be viewed as harmonically *sampling* an underlying formant envelope in the frequency domain. As the pitch of the source signal increases, this harmonic sampling becomes more sparse, thereby leading to a poorer spectral representation of the underlying formant envelope in the resulting spectrum [9]. Herein we discuss two realizations of a (2-D) analysis framework to address the spectral undersampling problem under certain conditions. Specifically, for a stationary formant envelope and *changing* pitch, we argue that spectral sampling can be improved. Similarly, in a second realization, we argue for source-filter separability in a transformed 2-D space.

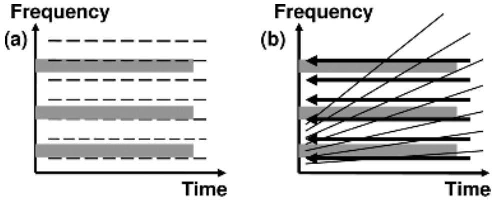

Fig. 2. Schematic of short-time Fourier transform of a stationary formant envelope (shaded) under conditions of (a) fixed pitch (dashed) and (b) changing pitch (solid). The black arrows indicate projection of spectral samples.

A. Harmonic Projection and Interpolation

Fig. 2 shows a schematic of a short-time Fourier transform (STFT) for a fixed vocal tract (shaded regions) under 1) fixed high-pitch (225 Hz) and 2) changing high-pitch conditions (200 to 250 Hz). As previously noted, a fixed high pitch results in spectral undersampling; we highlight these spectral samples in Fig. 3(b).[1] In contrast, consider now the STFT of the same vowel but with changing pitch from 200 Hz to 250 Hz; under a multiplicative source-filter model, the pitch harmonics sweep through the spectral envelope over time in a fan-like structure. To understand why this fan structure arises, consider a pitch f_0 with the nth and $(n+1)$th harmonics as nf_0 and $(n+1)f_0$, respectively. For a pitch change of Δf_0, the nth and $(n+1)$th harmonics of the new pitch $f_0 + \Delta f_0$ become $(f_0 + \Delta f_0)n$ and $(f_0 + \Delta f_0)(n+1)$, respectively. Whereas the nth harmonic is shifted by $\Delta f_0 n$, the $(n+1)$th harmonic is shifted by $\Delta f_0(n+1)$. Consequently, for a given Δf_0, higher-order harmonics are shifted more on an absolute frequency scale than lower-order harmonics. *A modest change in pitch shift can therefore invoke a substantial shift in increasing harmonic frequencies.* In the STFT, this results in fanning of the harmonic line structure at higher frequency regions [Fig. 2(b)].

Invoking now the spectral sampling from the pitch harmonics, multiple short-time spectral slices computed across time can therefore be viewed as a collection of nonuniform samples of the stationary spectral envelope for the condition of changing pitch. These samples can be projected [arrows, Fig. 2(b)] to the vertical frequency axis to provide improved sampling of

[1] Unless otherwise indicated, spectrograms plotted in this paper are on a linear scale.

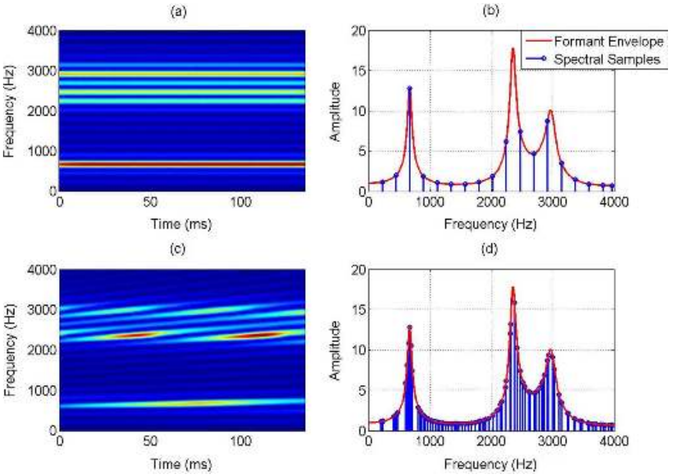

Fig. 3. (a) Pitch-adaptive spectrogram (Section II-B) of synthetic vowel with fixed pitch of 225 Hz. (b) Corresponding spectral samples of (a). (c) Pitch-adaptive spectrogram for synthetic vowel with moving pitch from 200 to 250 Hz; observe the fanning of the harmonic line structure as expected from Fig. 2(b). (d) Spectral samples from projection of changing pitch harmonics across time.

the underlying envelope. Fig. 3(c) shows an example of this increased sampling due to changing pitch, contrasting the uniform sampling in Fig. 3(b). A spectrum derived from this increased sampling could provide an improved representation of the underlying formant envelope especially under conditions of high pitch relative to that of a single spectral slice. Observe also that low-frequency regions (e.g., ~500 Hz) exhibit narrower sampling than the broader sampling in high-frequency regions (e.g., ~2000 Hz) due to the fanning of harmonic lines in higher-frequency regions (i.e., higher order harmonics).

For the subsequent discussions, our results involving harmonic projection are largely empirical. Note, however, that if additional samples from projection were to provide an increased density of *uniform* spectral samples, aliasing in the signal's corresponding autocorrelation function can be reduced and linear prediction all-pole modeling can be improved [5]. More generally, reconstruction methods from nonuniform samples exist in the literature (e.g., [13]), but are beyond the scope of this paper.

B. *Grating Compression Transform*

As another realization of the 2-D framework, we use an analysis scheme proposed by Quatieri in [1] and extended by Ezzat *et al.* in [2]. Specifically, the Grating Compression Transform (GCT) is defined as the 2-D Fourier transform computed over a spectrotemporally localized region of the STFT magnitude. The resulting 2-D space has been suggested to exhibit source-filter separability by Ezzat *et al.* through phenomenological analyses [2]. Herein we motivate analytically the GCT and propose a model for source-filter separability to support those observations.

1-D Modeling of Source: To motivate the GCT, we first consider a periodic impulse train in discrete time

$$p[n] = \sum_{k=-\infty}^{\infty} \delta[n - kN_0] \tag{1}$$

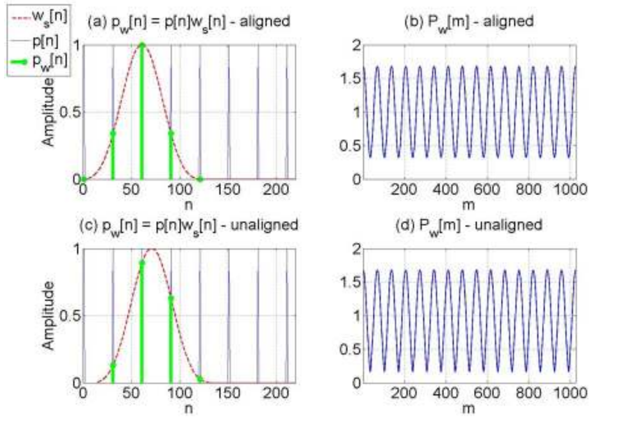

Fig. 4. (a) Windowing a periodic impulse train with pulse alignment. (b) Magnitude DFT of (a). (c) Windowing a periodic impulse train without alignment. (d) Magnitude DFT of (c).

with $N_0 = 30$ as shown in Fig. 4(a). Windowing $p[n]$ with a symmetric window $w_s[n] = w_s[N-n]$ results in the signal shown in Fig. 4(a). $w_s[n]$ is chosen to be a Blackman window with duration four times the periodicity of $p[n]$ such that $N = 4N_0 + 1 = 121$. This short-time pitch-adaptive scheme ensures that the window captures three impulses when the window center is aligned with an impulse and at most four impulses when it is not aligned since the window has zeros at its endpoints. Fig. 4(a) shows the condition when the center of $w_s[n]$ is aligned with an impulse such that the windowed signal $p_w[n]$ contains three impulses. By symmetry of the window, and denoting $\alpha = w_s[N_0], p_w[n]$ then becomes

$$p_w[n] = \delta[n - 2N_0] + \alpha\delta[n - N_0] + \alpha\delta[n - 3N_0]. \tag{2}$$

Fig. 4(b) shows the magnitude of the $N_{\mathrm{DFT}} = 2048$-point discrete Fourier transform (DFT) of $p_w[n]$ (denoted as $P_w[m]$)

$$\begin{aligned} P_w[m] &= \sum_{n=0}^{N-1} p_w[n] e^{-j\frac{2\pi mn}{N_{\mathrm{DFT}}}} \\ &= e^{-j\frac{2\pi m(2N_0)}{N_{\mathrm{DFT}}}} + \alpha e^{-j\frac{2\pi m N_0}{N_{\mathrm{DFT}}}} + \alpha e^{-j\frac{2\pi m(3N_0)}{N_{\mathrm{DFT}}}} \\ &= e^{-j\frac{\pi m N_0}{N_{\mathrm{DFT}}}} \left[1 + 2\alpha \cos\left(\frac{2\pi m N_0}{N_{\mathrm{DFT}}}\right)\right] \end{aligned} \tag{3}$$

such that

$$|P_w[m]| = 1 + 2\alpha \cos\left(\frac{2\pi m N_0}{N_{\mathrm{DFT}}}\right) \tag{4}$$

when $\alpha < 1/2$. Our analysis shows that under certain conditions, the short-time analysis scheme described results in a Fourier transform magnitude corresponding to a sinusoid resting on a DC pedestal. For our assumed values $N_0 = 30$ and $N_{\mathrm{DFT}} = 2048$, the period of $|P_w[m]|$ (denoted as γ_0) is $\gamma_0 \triangleq (N_{\mathrm{DFT}})/(N_0) \approx 68$.

Consider now the more general situation in which $w_s[n]$ is positioned such that it does not align with an impulse. In this case, $p_w[n]$ will correspond to four impulses with varying amplitudes as shown in Fig. 4(c), i.e.,

$$p_w[n] = \sum_{i=0}^{3} \alpha_i \delta[n - iN_0 - \Delta] \tag{5}$$

where $0 < \Delta < N_0$ corresponds to an offset based on the position of the window and α_i are the distinct amplitudes. Because the spacing *between* impulses in $p[n]$ is N_0, the corresponding $P_w[m]$ exhibits periodicity with spacing $\gamma_0 \approx 68$. In the case shown in Fig. 4(c), observe that $\alpha_1 > \alpha_2 > \alpha_0 > \alpha_3$ such that $P_w[m]$ can be written as

$$\begin{aligned} P_w[m] &= \alpha_0 e^{-j\frac{2\pi m}{N_{\mathrm{DFT}}}\Delta} + \alpha_1 e^{-j\frac{2\pi m}{N_{\mathrm{DFT}}}(\Delta+N_0)} \\ &\quad + \alpha_2 e^{-j\frac{2\pi m}{N_{\mathrm{DFT}}}(\Delta+2N_0)} + \alpha_3 e^{-j\frac{2\pi m}{N_{\mathrm{DFT}}}(\Delta+3N_0)} \\ &= e^{-j\frac{2\pi m}{N_{\mathrm{DFT}}}(\Delta+N_0)} \left[\alpha_1 + 2\alpha_0 \cos\left(\frac{2\pi m}{\gamma_0}\right)\right] \\ &\quad + (\alpha_2 - \alpha_0) e^{-j\frac{2\pi m}{N_{\mathrm{DFT}}}(\Delta+2N_0)} \\ &\quad + \alpha_3 e^{-j\frac{2\pi m}{N_{\mathrm{DFT}}}(\Delta+3N_0)}. \end{aligned} \tag{6}$$

The present derivation is similar to that of the aligned window but with the addition of two complex exponential terms. Fig. 4(d) shows $|P_w[m]|$ for this case; observe that despite the presence of these added terms, $|P_w[m]|$ is similar in shape to that of the ideal case with periodicity $\gamma_0 \approx 68$ as expected.

To quantitatively assess the effect of the exponential terms in (6), Fig. 5 compares the Fourier transform of the short-time spectra $P_w[m]$ for both the aligned and unaligned cases. We denote this transformed result as $P_w(\Omega)$

$$P_w(\Omega) = \sum_{m=0}^{N_{\mathrm{DFT}}} P_w[m] e^{-j\Omega m}. \tag{7}$$

In both cases, $|P_w(\Omega)|$ exhibits peaks at $\Omega = (2\pi N_0)/(N_{\mathrm{DFT}}) \approx 0.03\pi$, consistent with$P_w[m]$ being derived from a periodic sequence. For the aligned case, a single peak [solid arrow, Fig. 5(a)] at $\Omega \approx 0.03\pi$ can be observed in addition to the DC term in $|P_w(\Omega)|$, corresponding to a sinusoid resting on a DC pedestal. The unaligned case exhibits additional peaks at multiples of $\Omega \approx 0.03\pi$ as can be expected for a periodic sequence [e.g., dotted arrows, Fig. 5(b)]. Fig. 6(a) and (b) plot gives locations and amplitudes of the two largest non-DC peaks of $|P_w(\Omega)|$ for the unaligned case as a function of the window offset Δ. Observe that a dominant peak is consistently located at $\Omega \approx 0.03\pi$ while the secondary peak is located at $\Omega \approx 0.06\pi$.

Our analysis demonstrates that the maximum non-DC peak of $|P_w(\Omega)|$ is consistently located at a value corresponding to the pitch period of the signal, and that its magnitude tends to dominate $|P_w(\Omega)|$, *independent of the window alignment*. In our subsequent discussion, we approximate $|P_w(\Omega)|$ of the unaligned case as a sinusoid resting on a DC pedestal as in the aligned case.

One-Dimensional Modeling of Vocal Tract: The previous discussion has shown that for an appropriate choice of window, the Fourier transform of a windowed impulse train resembles a sinusoid resting on a DC pedestal. In the traditional source-filter production model, this impulse train is convolved with both glottal source and formant structure components to generate the speech signal. In accordance with this model, we view the sinusoid on a DC pedestal as corresponding to the periodic source component; in addition, for a *localized* frequency region, we view the source component as being *modulated* by a slowly-varying function corresponding to the local glottal source and formant structure spectral components. Let us denote $|X[m]|$ as the short-time magnitude spectrum computed using the previously described pitch-adaptive Blackman window. Denoting $a[m]$ as the envelope and $w[m]$ as a window along the frequency dimension, we model a local portion of the short-time magnitude spectrum as

$$\begin{aligned} |X_w[m]| &= w[m]a[m]\left[1 + \cos\left(\frac{2\pi m}{\gamma_0}\right)\right] \\ &= w[m]a[m] + a[m]w[m]\cos\left(\frac{2\pi m}{\gamma_0}\right) \end{aligned} \tag{8}$$

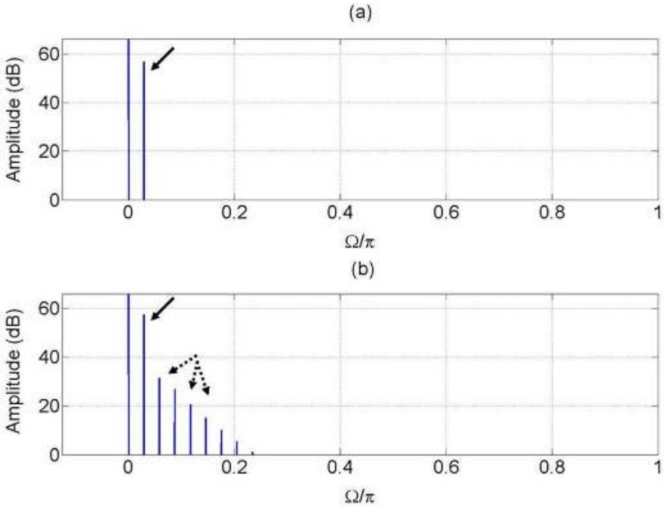

Fig. 5. (a) $|P_w(\Omega)|$ for aligned window. (b) $|P_w(\Omega)|$ for unaligned window; solid arrows denote $\Omega \approx 0.03\pi$ while the dotted arrows denote multiples of $\Omega \approx 0.03\pi$.

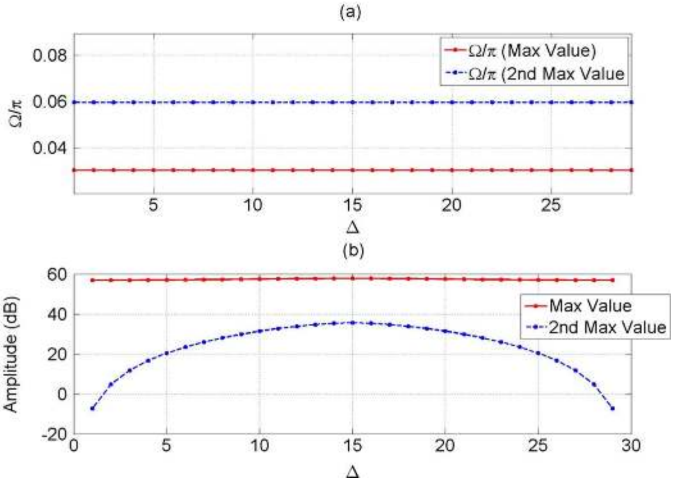

Fig. 6. (a) Location of two maximum non-DC peaks in $|P_w(\Omega)|$ for unaligned case. (b) Maximum values of two maximum non-DC peaks in $|P_w(\Omega)|$ for unaligned case.

where γ_0 is inversely proportional to the pitch. Denoting the Fourier transform of $|X_w[m]|$ as $X(\Omega)$, we have that

$$X(\Omega) = H(\Omega) + H\left(\Omega - \frac{2\pi}{\gamma_0}\right) + H\left(\Omega + \frac{2\pi}{\gamma_0}\right)$$
$$H(\Omega) = \frac{1}{2\pi} A(\Omega) *_{\Omega} W(\Omega) \tag{9}$$

where $A(\Omega)$ and $W(\Omega)$ are the Fourier transforms of $a[m]$ and $w[m]$, respectively, and $H(\Omega)$ is their convolution in the Ω domain.

In Fig. 7, we analyze a portion of the vowel /ae/ spoken by a female talker from the TIMIT corpus with pitch ~300 Hz; the sampling rate of the waveform is 8 kHz such that $N_0 \approx 27$. Fig. 7(a) shows the short-time magnitude spectrum $|X[m]|$ computed using a pitch-adaptive Blackman window and $N_{\mathrm{DFT}} = 2048$. Fig. 7(b) shows a localized frequency region of $|X_w[m]|$ to be analyzed. In absolute frequency, this region has size of ~700 Hz to capture approximately a single formant peak region as shown in Fig. 7(a) (rectangle). By low-pass filtering the corresponding $X(\Omega)$, we may recover and divide out the envelope $a[m]$ (Fig. 7(b), red solid) from $|X_w[m]|$. The filtering operation is done using a Hamming window with length corresponding to a low-pass[2] cutoff of $\Omega = (2\pi)/(\gamma_0) = (2\pi N_0)/(N_{\mathrm{DFT}}) = 0.026\pi$. The result of dividing out $a[m]$ from $|X_w[m]|$ is shown in Fig. 7(b) (magenta dashed). Observe that this result approximates the previously described sinusoid on a DC pedestal. In addition, Fig. 7(d) shows the Fourier transform magnitude computed for $(|X_w[m]|)/(a[m])$ after windowing with a Hamming window, which we denote as $P_{xa}(\Omega)$. Observe that a dominant peak at $\Omega \approx 0.026\pi$ can be observed, consistent with the sinewave model. As previously discussed, $|P_{xa}(\Omega)|$ may in general contain additional lower-amplitude peaks at multiples of $\Omega \approx 0.026\pi$ due to imperfect alignment of the short-time analysis window. Nonetheless, as will be subsequently discussed in Section III-B, these second peaks will have negligible effect on the GCT analysis method used in formant estimation.

Two-Dimensional Modeling of Source and Vocal Tract: The previous discussions invoke a 1-D modulation view of the short-time magnitude spectrum along the frequency dimension. This framework can be extended to include the time dimension of the STFT magnitude. Consider now a localized *spectrotemporal* region of the STFT magnitude obtained using a 2-D window [e.g., Fig. 8(a)]. Specifically, denote $s[n, m]$ as the STFT magnitude, $w[n, m]$ as the 2-D window, and the localized region centered at $n = n_0$ and $m = m_0$ as

$$s_w[n, m] = s[n, m] w[n - n_0, m - m_0]. \tag{10}$$

While a changing f_0 invokes a fanned harmonic line structure in $s[n, m]$, a localized region exhibits a harmonic line structure that is angled and approximately parallel as shown in Fig. 8(b) (solid lines). Likewise, a stationary pitch will invoke a set of horizontally-oriented parallel harmonic lines (dashed lines). Analogous to the 1-D case, we model the localized region as the product between a 2-D sinusoid resting on a DC pedestal with a slowly-varying envelope (denoted as $a[n, m]$) [9] such that $s_w[n, m]$ is

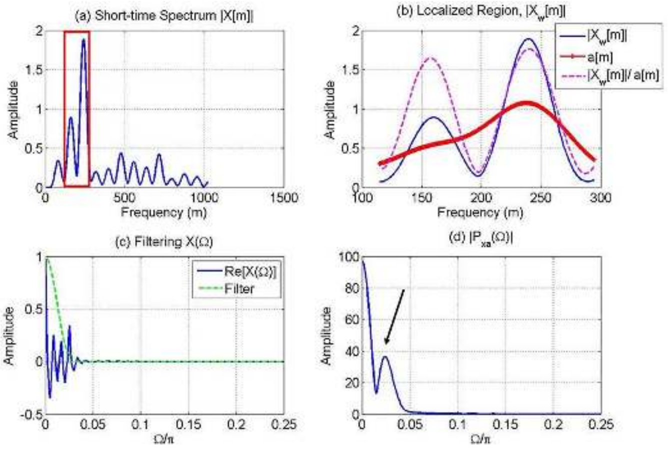

Fig. 7. (a) Short-time spectrum computed using pitch-adaptive analysis scheme and localized region to be analyzed (rectangle). (b) Localized region $|X[m]|$ with recovered envelope from filtering ($a[m]$, solid) and result of dividing $|X_w[m]|$ by $a[m]$ (dashed). (c) Filtering in the $X(\Omega)$ domain; note that only the real part of $X(\Omega)$ is shown (solid) along with the simple Hamming window filter (dashed). (d) Magnitude of $P_{xa}(\Omega)$; a dominant peak is located at $\Omega \approx 0.026\pi$ (arrow).

$$s_w[n, m] \approx w[n, m](1 + \cos(\omega_0 \Phi[n, m]))a[n, m] \tag{11}$$

where ω_0 is the spatial frequency of the 2-D sinusoid, and $\Phi[n, m]$ is defined as

$$\Phi[n, m] = m\cos(\theta) + n\sin(\theta) \tag{12}$$

corresponding to a term representing its spatial orientation. In relation to the traditional source-filter production model, we interpret $1 + \cos(\omega_0 \Phi[n, m])$ as a 2-D "source" component corresponding to harmonic line structure while $a[n, m]$ corresponds to a localized (in time *and* frequency) portion of the underlying vocal-tract formant excitation envelope. Expanding (11), we obtain

$$s_w[n, m] \approx w[n, m]a[n, m] + w[n, m]a[n, m]\cos(\omega_0 \Phi[n, m]) \tag{13}$$

such that the localized region is the *sum* of a slowly-varying component corresponding to the localized portion of the formant envelope with a modulated version of itself.

Applying the 2-D Fourier transform to $s_w[n, m]$ results in the GCT. Specifically, let N and M denote the time and frequency widths of the 2-D window, respectively; likewise, let ω and Ω denote the frequency variables corresponding to n and m, respectively. The GCT of $s_w[n, m]$ is defined as

$$S_w(\omega, \Omega) = \sum_{n=0}^{N-1} \sum_{m=0}^{M-1} s_w[n, m] e^{-j\omega n} e^{-j\Omega m}. \tag{14}$$

Substituting (13) into (14), we obtain

$$S_w(\omega, \Omega) \approx H(\omega, \Omega) + H(\omega + \omega_0 \sin\theta, \Omega - \omega_0 \cos\theta)$$
$$+ H(\omega - \omega_0 \sin\theta, \Omega + \omega_0 \sin\theta)$$
$$H(\omega, \Omega) \approx \frac{1}{2\pi} W(\omega, \Omega) *_{\omega,\Omega} A(\omega, \Omega). \tag{15}$$

[2] Although there are a number of methods for computing the spectral envelope, we do so here by low-pass filtering.

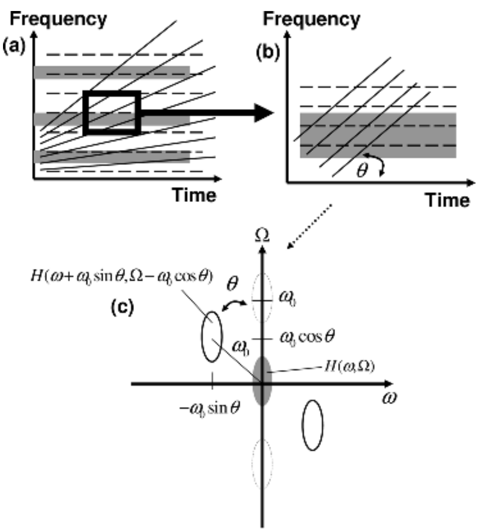

Fig. 8. (a) STFT and localized region (rectangle) used for GCT computation; stationary formant (shaded), fixed-pitch (dashed), and changing pitch (solid). (b) Localized region of STFT zoomed-in showing parallel harmonic line structure. (c) Grating Compression Transform of the modeled localized region of (11); observe the localized formant envelope is centered at the origin (shaded ellipse) while modulated versions of it are located ω_0 away from the origin at an angle θ off the Ω -axis depending on whether pitch is changing (solid ellipses) or fixed (dashed ellipses).

Fig. 8 shows a schematic of the mapping from $s_w[n,m]$ to $S_w(\omega,\Omega)$. We see that $w[n,m]a[n,m]$ maps to a function $H(\omega,\Omega)$ centered at the origin and oriented along the Ω-axis (represented schematically by the shaded ellipses) since the formant envelope is assumed to be stationary. The orientation of components in $S_w(\omega,\Omega)$ can be seen through basic properties of 2-D Fourier Transforms [14]. In contrast, $w[n,m]a[n,m]\cos(\omega_0\Phi[n,m])$ is transformed to a pair of smeared impulses located in opposed quadrants of the ω,Ω-plane due to the conjugate symmetric property of the 2-D Fourier transform. The radial distance between each smeared impulse and the GCT origin corresponds to the spatial frequency of the 2-D sinusoid (ω_0). When f_0 is fixed, the smeared impulses lie along the Ω-axis (dashed ellipses) (i.e., $\theta = 0$). For changing f_0, the rotational nature in transforming rotated harmonic lines maps them *off* the Ω-axis at a nonzero angle θ (solid ellipses). Our formulation therefore illustrates analytically the GCT's ability to invoke source-filter separability observed phenomenologically in [2]. Specifically, for fixed f_0, source-filter separability is invoked along the Ω-axis when ω_0 and the Ω-bandwidth of $H(\omega,\Omega)$ are such that there is minimal interaction between $H(\omega,\Omega)$ and $H(\omega,\Omega\pm\omega_0)$. For changing pitch, separability may be improved since the modulated version of $H(\omega,\Omega)$ is rotated off the Ω-axis, thereby reducing its interaction with the unmodulated $H(\omega,\Omega)$ oriented along the Ω-axis.

Observe that the separability invoked by the GCT is similar to that of the cepstrum [5]. Specifically, both analysis methods transform a multiplicative source-filter spectral model to an alternate domain where the source and filter are additive components; however, the GCT does so without invoking a homomorphic framework. In contrast to the cepstrum, the GCT can provide additional separability when f_0 is changing even under high-pitch conditions. Finally, observe that for changing f_0, harmonic lines in the STFT tend to fan out with greatest slope in high-frequency regions. The increased fanning corresponds to larger values of θ when mapped in the GCT. We therefore expect increased separability for these regions relative to lower frequency regions. This is analogous to the broader harmonic sampling discussed in Section II-A.

Our observations motivate a simple method for improving spectral representations of the formant structure in high-pitch speech to address spectral undersampling. Specifically, filtering in the GCT domain followed by an inverse 2-D Fourier transform can be used to generate a spectrum distinct from that obtained from a single spectral slice.

III. Formant Estimation Methodology

This section describes the methodology used in evaluating our 2-D processing framework for formant estimation. As discussed in Section I, we aim to directly assess the value of spectral representations obtained from different analysis methods and therefore obtain formant frequency estimates *directly* from the results of analysis (Fig. 1, *) rather than with a tracking mechanism. Herein we develop specific methods for obtaining spectral representations motivated from our observations presented in Section II. The resulting magnitude spectra are then used in linear prediction to estimate formant frequencies. In the development of these estimation methods, and later in Section IV, we use a series of synthesized vowels with varying amounts of linear pitch shifts. Finally two standard analysis methods, traditional and homomorphic linear prediction, are described, to be used as baselines in our comparative study in Section IV.

A. Vowel Synthesis

In this portion of our development, we use for a source signal in synthesis periodic impulse trains with varying degrees of pitch dynamics, thereby excluding the glottal pulse shape and its contribution to the speech spectrum. This is done to assess the benefits of exploiting pitch dynamics in high-pitch formant estimation with adequate compensation for this component. In our subsequent discussion of processing natural speech (Section V), we illustrate the feasibility of applying these methods to real and resynthesized speech using a simple compensation method.

Periodic impulse-train source signals with starting $f_0(f_{0s})$ ranging from 80–200 Hz (males), 150–350 Hz (females), and 200–450 Hz (children) were synthesized with linear pitch increases (df_0) ranging from 10 to 50 Hz. f_{0s} and df_0 varied in 5-Hz steps. Starting and ending pitch values were linearly interpolated across the duration of each synthesized utterance. To generate the impulse train with time-varying pitch, impulses were spaced according to this interpolation across the desired duration. Initially, we synthesized the source at 8 kHz; however, with this sampling rate, sharp transitions were observed in the spectrogram at pitch transition points, indicative of insufficient temporal resolution. To generate a smoother pitch track, we used instead a 96-kHz sampling rate for generating the impulse train and downsampled the result to 8 kHz, thereby minimizing these

TABLE I
AVERAGE VOWEL BANDWIDTHS USED IN SYNTHESIS (Hz)

	/ah/	/iy/	/ey/	/ae/	/oh/	/oo/
B1	60	38	42	65	47	50
B2	50	66	72	90	50	58
B3	102	171	126	156	98	107

TABLE II
AVERAGE VOWEL DURATIONS USED IN SYNTHESIS (ms)

	/ah/	/iy/	/ey/	/ae/	/oh/	/oo/
Duration	95	100	125	135	135	105

transitions. Due to the time-varying nature of the desired source signal and downsampling, the resulting source signal is not a periodic impulse train; however, the source signal was not observed to invoke significant spectral shaping to the vowel.

Source signals were filtered with sixth-order all-pole models [15] corresponding to the vowels /ah/ $(\mathrm{v} = 1)$, /iy/ (2), /ey/ (3), /ae/ (4), /oh/ (5), and /oo/ (6). Formant frequencies (F1, F2, F3) were set to average measurements reported by Hillenbrand *et al.* for males, females and children [16]. Formant bandwidths (B1, B2, B3) for all three genders were set to the average vowel-specific measurements made by Dunn listed in Table I [17]. Similarly, synthesized-utterance durations for all three genders were set to average measurements from the Switchboard corpus by Greenberg and Hitchcock and are listed in Table II [18].

B. Method of Harmonic Projection and Interpolation

To generate a magnitude spectrum using the projection and interpolation of harmonics (Fig. 2), we first used peak picking to obtain the harmonic peaks. Initially, we performed short-time analysis using a fixed 20-ms Hamming window. Fig. 9 (top) illustrates short-time spectra for the female vowel /ae/ across the minimum, average, and maximum pitch values used in synthesis. Observe that distinct mainlobes of the analysis window are located at harmonic frequencies of the pitch values for the 290- and 500-Hz pitch conditions; this is not the case for the 80-Hz pitch value due to the close proximity of the corresponding harmonics in the frequency domain. To address this, we used instead the pitch-adaptive short-time analysis scheme described in Section II such that larger pitch periods were analyzed with longer windows. Fig. 9 (bottom) shows spectra derived in this manner. Specifically, the Blackman window of length four times the pitch period was observed to provide reasonable harmonic peaks across all pitch conditions. The projection and interpolation method was therefore implemented according to the following steps:

1) an STFT was computed with a pitch-adaptive Blackman window $w_B[n]$ with length four times the pitch period at a 1-ms frame interval (STFT_1);
2) spectral slices of STFT_1 were scaled by $W_B(0) = \sum_{n=0}^{M-1} w_B[n]$;
3) peak-picking of the f_0 harmonics was performed across all normalized spectral slices of STFT_1 using the SEEVOC algorithm [19];
4) all harmonic peaks were collapsed into a single function and interpolated across frequency.

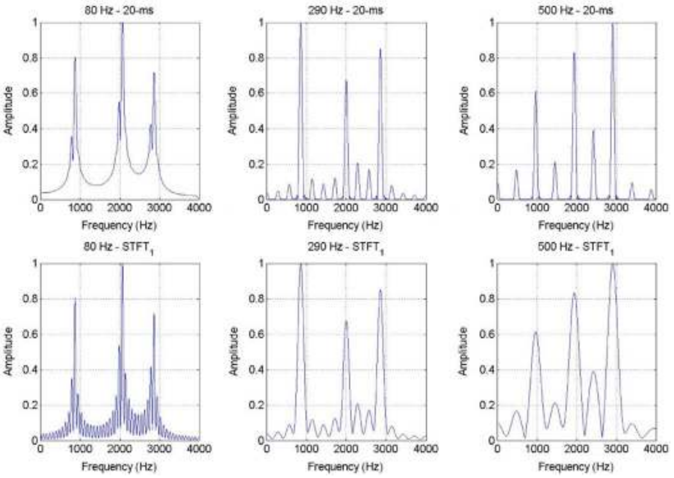

Fig. 9. Short-time analysis based on a fixed 20-ms Hamming window (top) versus pitch-adaptive Blackman window (bottom); observe that harmonic resolution is preserved in the latter method.

The value of f_0 used for the SEEVOC algorithm in Step 3 was obtained from the pitch contour used in synthesis. Due to the pitch-adaptive window, the corresponding short-time spectrum is scaled differently across frames since $W_B(0)$ is dependent on the window length. The harmonic peaks corresponding to portions of the formant envelope are therefore scaled by $W_B(0)$ to invoke the same absolute magnitudes across spectral slices, independent of window length (Step 2). In Fig. 10(a), we show the pitch-adaptive spectrogram while Fig. 10(b) illustrates peak-picking using the SEEVOC algorithm. Interpolation across the harmonic peaks using a shape-preserving piecewise cubic interpolator [20] was performed to obtain a smooth spectrum. Fig. 10(c) shows the collection of harmonic samples obtained across the entire vowel and the interpolated magnitude spectrum. We denote this method as $m3$. Finally, to remove confounds of the interpolation method itself, interpolation was also performed on harmonic spectral samples from a single spectral slice of STFT_1 extracted from the middle of the utterance $(m4)$. The resulting single-slice interpolation is shown in Fig. 10(b).

In addition to $m3$, we also implemented a simpler method of projection and interpolation by computing the average (across time) of all spectral slices of STFT_1 which we denote as $m5$. Fig. 10(d) shows the result of averaging all magnitude spectral slices in STFT_1 (solid) along with two sample spectral slices (dashed) used in computing this average. This method can also be thought of in the context of the GCT; specifically, it can be easily shown that this method is equivalent to extracting the Ω-axis of the GCT computed for localized regions of STFT_1 followed by an inverse Fourier transform.

C. Filtering the Grating Compression Transform

For method $m6$, we implemented filtering of the GCT based on the model of Section II-B. As previously discussed in Section II, the pitch-adaptive short-time analysis used for $m3$ through $m5$ provides a reasonable correspondence to the model invoked by the GCT. Specifically, localized frequency regions approximately resemble a sinusoid on a DC pedestal modulated by a slowly-varying function (as in Fig. 7) across pitch conditions in Fig. 9. For method $m6$, localized regions (denoted

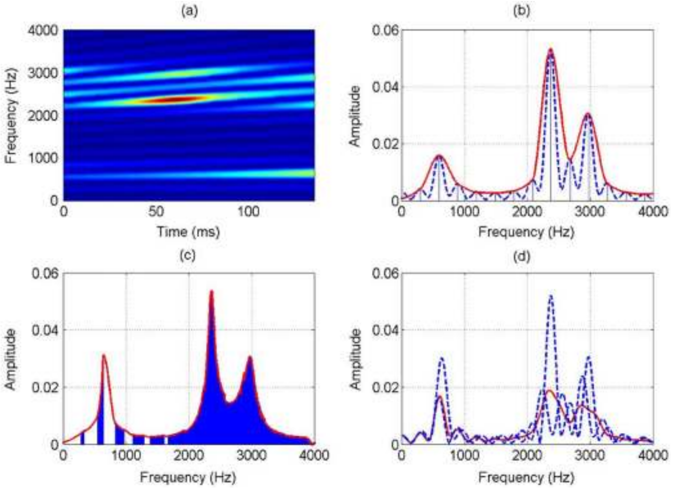

Fig. 10. Harmonic projection and interpolation applied to vowel with time-varying pitch. (a) Pitch-adaptive short-time spectrogram (STFT_1). (b) Single-slice (spectral slice, dashed) peak-picking using SEEVOC algorithm (peaks, vertical stem) at 296 Hz and single-slice interpolation ($m4$, solid). (c) Projection of collected harmonic peaks across STFT_1 (peaks, vertical stem) and interpolated spectral envelope ($m3$, solid). (d) Representative short-time spectra (dashed) used in the computing the resulting average spectrum ($m5$, solid).

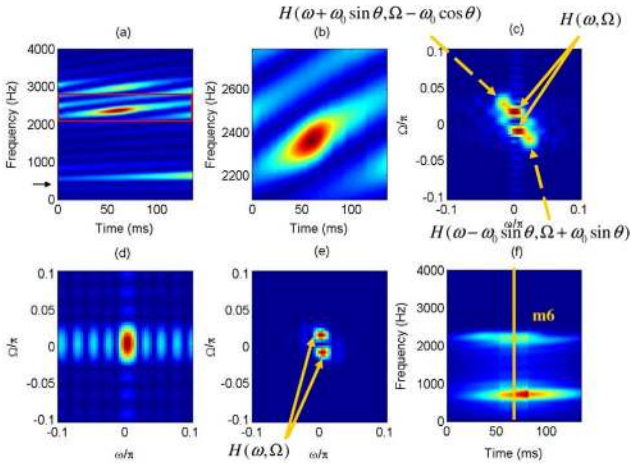

Fig. 11. Filtering in the GCT. (a) STFT and localized region (rectangle) used for computing the GCT; arrow denotes 350 Hz. (b) Zoomed-in localized region from (a). (c) $|\mathrm{GCT}_2|$ showing source-filter separation. *For display purposes only, the DC component has been removed*; note that this gives a null at the GCT origin that is not reflected in the schematic of Fig. 5. (d) 2-D filter applied to GCT_2. (e) Filtered version of GCT_2 (magnitude only); observe the absence of harmonic components off the Ω-axis. (f) Reconstructed time–frequency reconstruction; line denotes spectral slice extracted ($m6$).

as $s[n,m]$) were extracted from STFT_1 with a separable 2-D window $w[n,m]$. In time, we chose a rectangular window spanning the full duration of the vowel; in frequency, we used a 700-Hz Hamming window. Since the filtering operation is adaptive across frequency regions, a 350-Hz overlap across regions was invoked to reduce the effects of abrupt changes in the filter.

Two distinct GCTs were computed for each localized region: GCT_1 is used to perform peak-picking in estimating the local spatial frequency (ω_0) of the sinusoid due to harmonic structure, while GCT_2 is used to generate a spectral representation by filtering in the GCT domain. For GCT_1, a 2-D gradient operator of the matrix form [14]

$$\begin{bmatrix} 0 & 2 & 2 \\ -2 & 0 & 2 \\ -2 & -2 & 0 \end{bmatrix} \tag{16}$$

was applied to the entire STFT followed by removal of the DC component, prior to windowing and computing the 2-D Fourier transform. These operations were observed to reduce the magnitude of components near the GCT origin such that ω_0 could be estimated using a simple peak picker [1], [21]. For GCT_2, the DFT was computed directly from the windowed region without application of the 2-D gradient operation and DC removal

$$p_2[n,m] = w[n-n_0, m-m_0]s[n,m]$$
$$\mathrm{GCT}_2(\omega,\Omega) = \sum_{n=0}^{N-1}\sum_{m=0}^{M-1} p_2[n,m]e^{-j\omega n}e^{-j\Omega m}. \tag{17}$$

GCT_2 is filtered with an adaptive 2-D elliptic filter and reconstructed to generate a time–frequency distribution as illustrated through the example in Fig. 11. The 2-D filter was designed by taking the product of two linear-phase low-pass filters in frequency. In time, the pass and stop band edges were fixed to $0.25\omega_l$ and $0.5\omega_l$, respectively. ω_l corresponds to the ω_0 estimate derived from the lowest frequency region of STFT_1 with center frequency of 350 Hz (arrow, Fig. 11(a)). In frequency, we used pass and stop band edges of $0.25\omega_0$ and ω_0, respectively, with ω_0 corresponding to the local estimate for each region. The filter cutoffs were motivated from empirical observations showing that ω_0 tended to increase with frequency region. This effect is caused by the increased fanning of the harmonic line structure towards high-frequency regions; because the harmonic lines are no longer strictly parallel, ω_0 was observed to be slightly overestimated in these regions. Using the described filter cutoffs, we therefore obtain an adaptive low-pass elliptical filter that becomes more permissive along the Ω-direction for regions with increasing frequency, thereby allowing an improved recovery of $a[n,m]$ in each localized region. This is consistent with the improved source-filter separation in high-frequency regions previously discussed in Section II-B.

As shown in Fig. 11(e), filtering of GCT_2 removes the modulated versions of the localized formant envelope $H(\omega \pm \omega_0 \sin\theta, \Omega \mp \omega_0 \cos\theta)$, thereby leaving only the unmodulated version $H(\omega,\Omega)$. Note that while we show only the magnitudes of the GCT in Fig. 11, filtering was done on the *complex* GCT_2. To generate the magnitude spectrum for comparison with other methods, a reconstructed time–frequency distribution (Fig. 11(f)) was computed using overlap-add, and a spectral slice was extracted corresponding in time to the middle of the utterance. Finally, recall from Section II-B. that the approximate sinusoidal model can exhibit harmonic peaks in the GCT domain at multiples of the local spatial frequency. Nonetheless, since the current method extracts formant information near the GCT *origin* using the low-pass filter, these peaks will have negligible effect on the resulting reconstruction.

D. Baseline Methods

Two baseline methods were implemented for comparison with those aiming to exploit temporal change of pitch. Specifically, a magnitude STFT (denoted as STFT_0) was computed for each utterance using a 20-ms Hamming window, 1-ms

TABLE III
SUMMARY OF FORMANT ESTIMATION METHODS

m1	Traditional Linear Prediction (LP)
m2	Homomorphic Linear Prediction
m3	Harmonic Projection and Interpolation + LP
m4	Single-slice Projection and Interpolation + LP
m5	Spectral Slice Averaging + LP
m6	GCT Filtering + LP

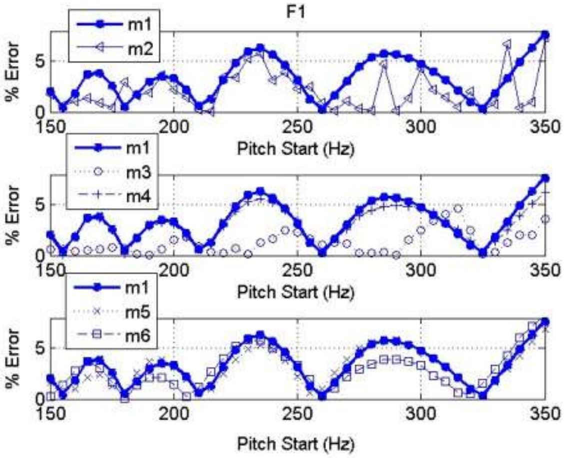

Fig. 12. Raw percent formant error for female /ae/ F1.

frame interval, and 2048-point DFT. A single spectral slice located in the middle of the utterance (denoted as $|X_{\mathrm{STFT}_0}[k]|$) was then extracted for use with linear prediction; we refer to this as traditional linear prediction $(m1)$.

As another reference, we performed homomorphic linear prediction on $|X_{\mathrm{STFT}_0}[k]|$. Specifically, Rahman and Shimamura have suggested the computation of the real-cepstrum

$$c_{\mathrm{STFT}_0}[n] = \frac{1}{N}\sum_{k=0}^{N-1} \log |X_{\mathrm{STFT}_0}[k]| e^{j\frac{2\pi kn}{N}} \tag{18}$$

followed by liftering with an ideal lifter with cutoff $(0.6)/(f_0)$ for $f_0 \leq 250$ Hz and $(0.7)/(f_0)$ for $f_0 > 250$ Hz $(N = 2048)$ [22]. As in method $m3$, f_0 was obtained from the pitch contour used in synthesis. The DFT was then computed to generate a magnitude spectrum to be used with linear prediction.

E. Autocorrelation Method of Linear Prediction

For formant estimation, the one-sided magnitude spectra resulting from methods $m1$ through $m6$ (denoted as $|X[k]|$) are used to obtain autocorrelation estimates for use in linear prediction. Specifically, $|X[k]|$ is appended by a frequency-reversed version, thereby resulting in a two-sided zero-phase spectrum denoted as $X_2[k]$. The inverse DFT of $X_2^2[k]$ provides the autocorrelation estimate $r_x[n]$. $r_x[n]$ is then used to generate the normal equations which are then solved using the Levinson–Durbin recursion [23]. Recall from our discussion in Section III-A that we used as the vocal tract source signal a downsampled periodic impulse train to eliminate the effects of spectral tilt due to the glottal waveform present in natural speech. The model order was therefore set to 6 to correspond directly to the three synthesized formants. Finally, the roots of the resulting coefficients from linear prediction are solved to obtain the formant frequency estimates for all spectral representations.

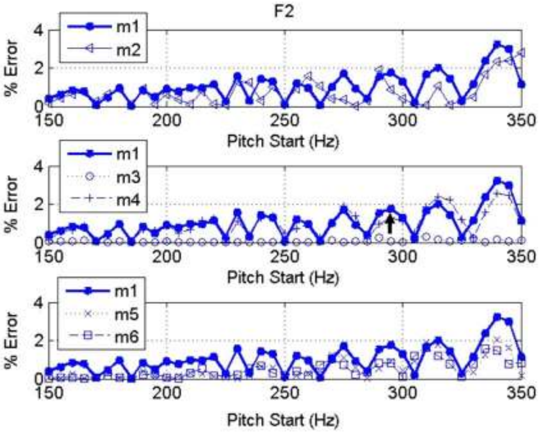

Fig. 13. Raw percent formant error for female /ae/, F2. Arrow denotes a relative comparison between m3 and m1 for a pitch start of 295 Hz.

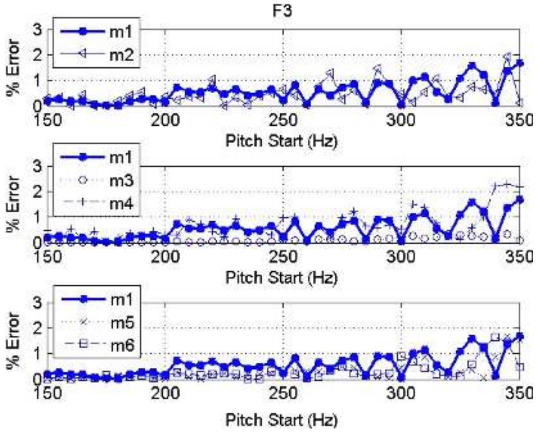

Fig. 14. Raw percent formant error for female /ae/, F3.

IV. RESULTS ON SYNTHETIC VOWELS

This section compares the results of formant estimation using methods $m1$ through $m6$ in the experimental setup described in Section III on synthetic vowels. Table III lists the methods to be compared. We use as a metric the absolute percent error between an estimated $(\hat{F})$ versus the true (F) formant-frequency value:

$$\%\mathrm{error} = 100\frac{|\hat{F} - F|}{F}. \tag{19}$$

A. Raw Percent Error

For the ith formant of the vth vowel with df_0 pitch shift, starting pitch f_{0s}, and gender g, the raw percent error using method m is defined as

$$E_g(i, v, df_0, f_{0s}; m) = 100\frac{|\hat{F}_g(i, v, df_0, f_{0s}; m) - F_g(i, v)|}{F_g(i, v)}. \tag{20}$$

$F_g(i, v)$ corresponds to the true ith formant frequency of the vth vowel for gender g while $\hat{F}_g(i, v, df_0, f_{0s}; m)$ corresponds to the estimate using method m. Figs. 12–14 show representative results across methods and formant number for the female vowel

/ae/ with $df_0 = 25$ Hz; in this case, (20) can be viewed as a function of the pitch start (f_{0s}).

Some preliminary observations can be made for the traditional linear prediction baseline ($m1$, Figs. 12–14). Recall that we use for analysis a 20-ms Hamming window and a sixth-order linear prediction estimate. We observe that errors exhibit an oscillatory behavior across f_{0s}; in addition, the rate of oscillations tends to increase with formant number, with the fastest oscillations occurring for F3. These observations are consistent with those observed by Vallabha and Tuller and may be explained by the alignment of pitch harmonics near (for local error minima) and away from (for local error maxima) formant peaks [24]; we refer to this explanation as "fortuitous sampling." In accordance with this explanation, pitch changes will invoke greater absolute changes in harmonic positions for higher frequency regions than lower regions such that F3 errors would be expected to oscillate more than F1 errors. Finally, observe that the size of oscillations increases with f_{0s}, consistent with the effect of spectral undersampling for higher-pitch formants.

Our results for homomorphic linear prediction $(m2)$ are consistent with those reported in [22] in providing gains over traditional linear prediction under some conditions (e.g., $\mathrm{F1} - f_{0s} = 295$ Hz). Nonetheless, observe that harmonic projection and interpolation $(m3)$ affords substantial error reductions over $m1$ and $m2$. In addition, the similarity between the errors invoked with single-slice interpolation $(m4)$ and $m1$ in this particular case suggest that the error reduction via $m3$ is due to exploiting temporal change of pitch rather than the interpolation method itself. Similarly, $m5$ and $m6$ also afford reductions in the error magnitude under certain conditions (e.g., F2, $m6$). These results suggest that exploiting temporal change of pitch can improve formant estimation for both low- and high-pitch conditions.

Observe that $m2, m3, m5$, and $m6$ exhibit some oscillatory behavior similar to $m1$; however, the local maxima of these oscillations can be lower than those of $m1$ (e.g., $m3$, all formants). For $m2, m3$, and $m5$, we interpret this effect in relation to the "fortuitous sampling" explanation of the oscillatory behavior as increasing the chances of harmonic peaks to align with formant peaks. Nonetheless, this is achieved differently between the methods. Whereas cepstral liftering smooths a spectrum *across frequencies* and can therefore distribute energy towards the true formant peaks, the projection and interpolation of harmonics does so *across time*. It appears that the latter method outperforms the former for this purpose (e.g., compare the peak errors for F2 between $m2$ and $m3$). For $m6$, we attribute the reduction in oscillation amplitude (e.g., for F2 and F3) to the improved source-filter separability invoked in transformed 2-D space.

B. Global Average

To assess the performance of methods across all synthesis conditions (i.e., vowel, pitch shifts, pitch starts), we computed a global average metric defined as

$$F_{i,m} = \frac{100}{SDV} \sum_{s=1}^{S} \sum_{d=1}^{D} \sum_{v=1}^{V} |\hat{F}_{i,m,s,d,v} - F_i^v| / F_i^v \qquad (21)$$

with S, D, and V corresponding to the total number of f_{0s}, df_0, and vowels, respectively. In addition, F_i^v corresponds to the true ith formant frequency for the vth vowel while $\hat{F}_{i,m,s,d,v}$ is its corresponding estimate for sth starting f_{0s} and dth df_0.

TABLE IV
GLOBAL AVERAGE OF RAW FORMANT %ERRORS FOR MALES, FEMALES, AND CHILDREN

	MALES	FEMALES	CHILDREN
F1	2.92	4.85	5.64
F2	0.84	1.58	1.89
F3	0.25	0.66	0.97

Table IV gives values of this global average for males, females, and children using the traditional linear prediction $(m1)$. Observe that the average error tends to increase from males, females, to children, consistent with the effects of increased spectral undersampling for the higher pitch females and children. Figs. 15–17 show the relative gains of all other methods with respect to this baseline and is computed as

$$\mathrm{RG}_{i,m'} = 100 \frac{F_{i,m1} - F_{i,m'}}{F_{i,m1}} \qquad (22)$$

for each gender; here, m' denotes the methods $m2$ through $m6$.

Overall, these results are consistent with those observed for the example discussed in Section IV-A. Harmonic projection and interpolation $(m3)$ exhibits the best performance with relative gains up ~83% for F3; in addition, relative losses incurred by single-slice interpolation $(m4)$ are consistent with the role of changing pitch in improving formant estimation (rather than the interpolation method itself). Spectral slice averaging $(m5)$ and filtering in the GCT $(m6)$ also exhibit similar gains over $m1$ in all conditions. In addition, they provide gains over $m2$ for F2 and F3 in males and females and F3 in children.

The similar performance of $m5$ and $m6$ is not entirely surprising, as we previously saw that the averaging method can be thought of in the context of the GCT (Section III-B). We believe that $m5$ and $m6$'s relatively smaller gains with respect to $m2$ for F1 stem from the reduced fanning of harmonic lines in lower frequency regions of the STFT. These are more likely to be mapped along the Ω-axis in the GCT, thereby reducing source-filter separability. In conjunction with the exceptionally high-pitch source signals used for synthesizing children's speech, this effect could also account for the relatively smaller gains in F2 for children using $m5$ and $m6$. Conversely, $m3, m5$, and $m6$ generally exhibit the larger gains for higher formants (e.g., F3) than lower formants, presumably due to broader harmonic sampling for $m3$ and $m5$ and the increased source-filter separability in the GCT for $m6$ in high-frequency regions.

V. MONOPHTHONG VOWELS IN NATURAL SPEECH

In this section, we illustrate the feasibility of applying the proposed methods for natural speech. As in Section III, we focus on the *analysis framework* for estimating formants rather than perform formant *tracking*. Specifically, we apply the proposed formant estimation methods discussed in Section III to real vowels spoken by high-pitch female talkers of the TIMIT corpus [12]. The vowels analyzed were extracted from TIMIT based on the available phone transcriptions and correspond

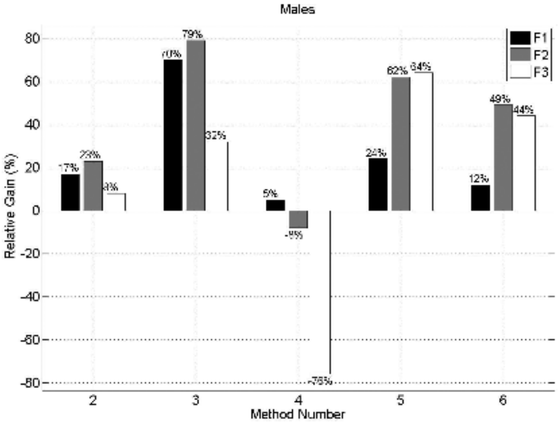

Fig. 15. Relative gains of $m2$ through $m6$ with respect to $m1$ for males.

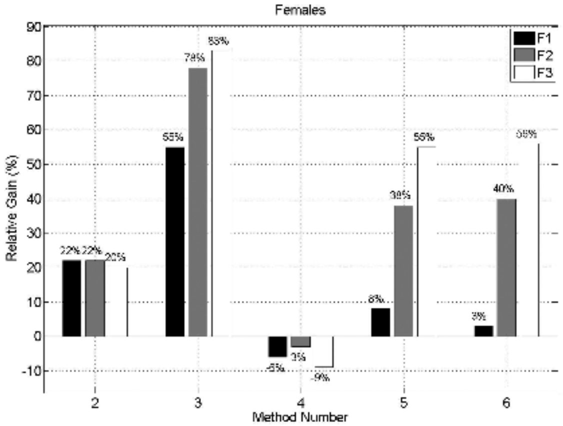

Fig. 16. Relative gains of $m2$ through $m6$ with respect to $m1$ for females.

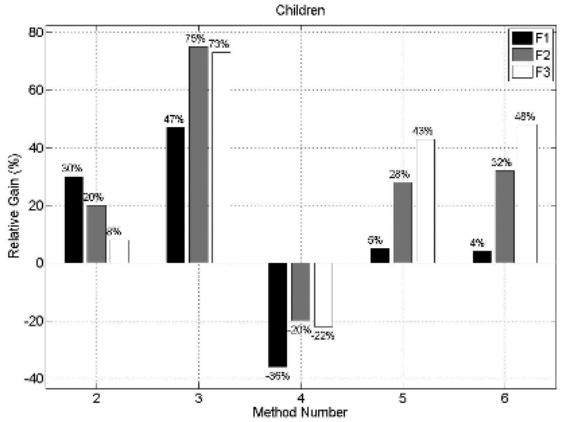

Fig. 17. Relative gains of $m2$ through $m6$ with respect to $m1$ for children.

to *monophthong* vowels (i.e., those with stationary or near stationary vocal tract configurations). While it is likely that the TIMIT transcriptions correspond to vowel regions in which the vocal tract is not strictly stationary, we believe this to be a reasonable approximation to demonstrate that 1) sufficient pitch variations are available in natural speech and 2) can occur in regions of stationary or near-stationary vocal tract configurations to be exploited by our methods. Two sets of analyses were performed for each vowel. In the first, we applied our methods directly to the natural speech. In the second, we estimate a set of reference formant frequencies from the natural speech and apply our methods to a *resynthesized* vowel. Herein we discuss the motivation, methodology, and results of our analyses.

A. Real Vowels

Monophthong vowel regions were extracted from TIMIT waveforms based on the available phone transcriptions. The autocorrelation-based pitch tracker of the Praat software package was employed using a 1-ms frame interval to estimate pitch values across each vowel's duration [25]. As a preprocessing step to methods $m1$ through $m6$, we applied a simple method of spectral tilt compensation to reduce the glottal source contribution to the speech spectrum present in natural speech. Specifically, the real cepstrum of STFT_1 was computed and the first (non-DC) cepstral coefficient was set to zero. This operation has the effect of removing a spectral tilt as derived from the real cepstrum at quefrency $\mathrm{n} = 1$ [5]. The modified STFT_1 was then obtained using the inverse transform and methods $m1$ through $m6$ were invoked as previously described in Section III. For the analysis of natural speech, reference formant frequencies have been proposed by Deng *et al.* in [26]. In that work, an initial set of formant values were estimated using an automatic formant tracking system. These values were then manually corrected to compensate for errors made by the formant tracker, particularly in regions of rapid formant transitions. However, because the ground truth formant values were derived in part using linear predictive cepstral coefficients (LPCC) in conjunction with a tracking mechanism, we are not able to use these as an appropriate reference for comparing against *non*-LPCC analysis methods (e.g., harmonic projection, GCT-based filtering). The results of our analysis for natural speech therefore serve primarily to illustrate differences in estimation results between the proposed methods and those of standard techniques. In contrast, our use of resynthesized vowels provide reference formant values not derived from LPCC-based estimation.

B. Resynthesized Vowels

In our second set of analyses, we aimed first to obtain a set of reference formant frequency values for use in *resynthesis* followed by the application of $m1$ through $m6$ on the resynthesized vowel. As was previously discussed, one aim of this experimental setup is to assess whether sufficient pitch dynamics are present in natural speech during stationary vowels such that the proposed methods can provide improvements over traditional methods. As a secondary aim for assessing feasibility of our methods for natural speech, recall from Section IV that our synthetic experiments used a periodic impulse train for a source signal, thereby excluding the glottal pulse shape's contribution to the speech spectrum in natural speech. This was done to illustrate the benefits of exploiting pitch dynamics in formant estimation if this component can be adequately removed. In this section, we instead incorporate a glottal pulse shape in resynthesis followed by the previously discussed cepstrum-based method of compensation in Section VI-A. While a variety of techniques in the literature (e.g., [27]) exist for spectral tilt compensation, our aim here is to assess the feasibility of employing the proposed methods in

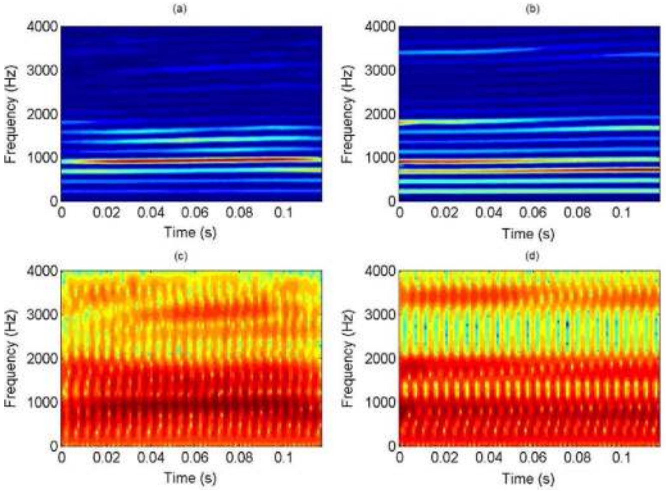

Fig. 18. (a), (c) Narrowband and log broadband spectrograms of real vowel. /ah/ extracted from female TIMIT speaker. (b), (d) Narrowband and broadband spectrograms for resynthesized vowel from estimated reference formant frequency values: $\mathrm{F1} = 374$ Hz, $\mathrm{F2} = 2315$ Hz, $\mathrm{F3} = 2835$ Hz. The pitch of the speaker ranged from 171–159 Hz throughout the vowel. The narrowband and broadband spectrograms were computed using a 20- and 5-ms Hamming window, respectively, at a 1-ms frame interval.

formant estimation in conjunction with a simple, though likely *incomplete*, compensation method.

To obtain a set of reference formant frequencies from the extracted vowel, we reasoned that the spectral slice corresponding to the lowest f_0 value in the vowel would be less likely to suffer from spectral undersampling. From the previous section, the spectral slice corresponding to the lowest f_0 of the modified STFT_1 was therefore used to estimate a set of reference formant frequencies via traditional linear prediction (i.e., $m1$). These values were used in conjunction with the formant bandwidths of Table I to specify an all-pole model as described in Section III; therefore, in the resynthesized vowels, we define these reference formant frequency values as ground truth. To generate the source signal for resynthesis, we used the estimated pitch contour to determine pulse periodicity as in Section IV; however, instead of a periodic impulse as in Section III, we used in this section the derivative of the Rosenberg model to invoke a glottal pulse shape [28]; the derivative was invoked to account for the radiation characteristics at the lips [29]. The resynthesized vowel was then analyzed by methods $m1$ through $m6$ in conjunction with the cepstrum-based method of spectral tilt compensation.

C. Results

In Fig. 18, we show an example of a real and resynthesized vowel /ah/ from a female TIMIT speaker. Both the narrowband (a,b) and log broadband (c,d) spectrograms are shown to emphasize harmonic and formant structure, respectively. Observe from the broadband spectrogram for the real vowel that F3 exhibits some movement at the beginning of vowel (e.g., near 0.02 s). Nonetheless, the formant structure appears stationary for the majority of the vowel duration. The pitch variation throughout the vowel increases from 251 to 278 Hz. Table V (top) lists the formant frequency estimates of the real vowel using $m1$ through $m6$ as well as the raw percent errors computed with respect to the reference formant frequencies on the resynthesized vowel for $m1$ through $m6$ (bottom). Similar sets of results are presented in Tables VI–VIII for /iy/, /ey/, and /ae/.

TABLE V
/ah/, PITCH VARIATION −251 TO 278 Hz

Estimates of $m1$ through $m6$ on natural speech utterance (Hz)							
	$m1$	$m2$	$m3$	$m4$	$m5$	$m6$	Truth (Hz)
F1	984	1132	966	1062	978	1002	-
F2	1551	1470	1707	1579	1695	1702	-
F3	3098	3173	3197	3113	3239	3219	-
Raw % errors of $m1$ through $m6$ on resynthesized vowel.							Truth (Hz)
F1	16.08	14.62	12.02	15.08	14.54	12.15	824
F2	1.08	0.85	0.56	0.41	0.18	0.78	1752
F3	0.81	1.17	0.07	0.9	0.01	0.08	3408

TABLE VI
/iy/, PITCH VARIATION −171 TO 150 Hz

Estimates of $m1$ through $m6$ on natural speech utterance (Hz)							
	$m1$	$m2$	$m3$	$m4$	$m5$	$m6$	Truth (Hz)
F1	399	411	413	401	394	408	-
F2	2392	2407	2381	2392	2366	2353	-
F3	2978	2983	2932	2984	2951	2934	-
Raw % errors of $m1$ through $m6$ on resynthesized vowel.							Truth (Hz)
F1	11.49	18.18	8.16	12.68	11.3	10.07	374
F2	2.21	1.65	0.77	2.00	0.91	0.91	2315
F3	1.85	1.62	1.09	1.59	1.42	1.19	2385

TABLE VII
/ey/, PITCH VARIATION −275 TO 205 Hz

Estimates of $m1$ through $m6$ on natural speech utterance (Hz)							
	$m1$	$m2$	$m3$	$m4$	$m5$	$m6$	Truth (Hz)
F1	468	433	580	475	520	496	-
F2	2505	2512	2457	2515	2441	2459	-
F3	2974	3042	2969	3020	3001	2943	-
Raw % errors of $m1$ through $m6$ on resynthesized vowel.							Truth (Hz)
F1	18.71	19.05	7.43	18.77	11.72	12.55	564
F2	0.57	0.41	0.1	0.66	0.04	0.03	2322
F3	0.71	0.64	0.29	0.48	0.44	0.30	2912

TABLE VIII
/ae/, PITCH VARIATION −245 TO 213 Hz

Estimates of $m1$ through $m6$ on natural speech utterance (Hz)							
	$m1$	$m2$	$m3$	$m4$	$m5$	$m6$	Truth (Hz)
F1	709	718	711	716	704	727	-
F2	2206	2223	2161	2247	2143	2129	-
F3	3052	3086	3075	3079	3095	3103	-
Raw % errors of $m1$ through $m6$ on resynthesized vowel.							Truth (Hz)
F1	15.30	14.61	7.52	16.03	13.02	13.57	732
F2	2.25	1.93	0.36	2.37	1.64	1.66	1912
F3	1.08	1.21	0.40	1.07	0.86	0.75	3232

The results of our analysis on natural speech show that the proposed methods provide estimates distinct from traditional and homomorphic linear prediction ($m1$ and $m2$). In addition, observe for the resynthesized vowels that the methods $m3, m5$, and $m6$ exhibit smaller percent errors from the reference formant frequencies than $m1$ and $m2$. These results illustrate that sufficient pitch variations are available in natural speech which can be exploited in improving formant estimation accuracy over traditional methods. In addition, the results illustrate the feasibility of applying the proposed methods in conjunction with a relatively simple spectral tilt compensation method in the presence of a glottal pulse shape.

VI. Implications for Formant Tracking

In this section, we demonstrate and discuss implications of the proposed analysis framework for the formant tracking problem. As previously noted, current state-of-the-art systems typically employ linear predictive cepstral coefficients (LPCC) in conjunction with a tracking mechanism (e.g., Kalman filtering [4], [30]) to obtain formant estimates across time. In particular, LPCCs are modeled as noisy observations corresponding to an unobserved state (the desired formant frequencies) to be estimated. Our previous results, however, have shown that traditional and homomorphic linear prediction, from which LPCCs are obtained, invoke poorer representations of stationary formant structure compared to analysis methods aiming to exploit temporal pitch dynamics. Herein we demonstrate through examples the effect that such representations have in formant estimation in stationary vowels in the context of formant tracking (i.e., the final output in the scheme of Fig. 1).

For our experimental framework, we applied the baseline extended Kalman filter (EKF) proposed originally in [4] and extended in [30] to synthetic vowels using different analysis methods for generating observations. State variables were chosen to be the three formant frequencies of the synthesized vowel and initialized to the reference formant frequencies. Formant bandwidths were also initialized and held fixed to the true bandwidths across state estimates in applying the EKF equations.

As a baseline observation type, we used 15th-order LPCCs computed for a 20-ms window of the speech signal computed at a 10-ms frame interval as in [30]. To exploit temporal pitch dynamics in generating observations, we applied the harmonic projection, averaging, and GCT-based analysis methods previously described to generate short-time spectral representations; these estimates were subsequently used to obtain 15th-order LPCCs to be used as observations in the EKF. For averaging, collections of spectral slices from STFT_1 spanning 20-ms durations (20 slices total) were extracted at 10-ms intervals and averaged. For harmonic projection, these same spectral slices were used in peak-picking, projection to a single axis, and interpolation to generate a spectral representation as described in Section III; in addition, a control estimate of peak-picking and interpolation using peaks of a *single* slice was computed. For GCT-based analysis, the adaptive 2-D elliptical filter described in Section III was applied across regions of STFT_1 of size 700 Hz by 20 ms using a 2-D Hamming window. For overlap-add, overlaps of 350 Hz and 10 ms were invoked in frequency and time, respectively. This is in contrast to the GCT-based analysis in Section III that used the full duration of the vowel. Finally, spectral slices were extracted from the filtered spectrogram at 10-ms intervals to generate the desired LPCC observations.

Figs. 19 and 20 show results of the tracker for a synthetic female vowel /ae/ with pitch ranging from 150 to 200 Hz and 250 to 300 Hz, respectively. The baseline LPCC observation results in errors in frequency estimates ranging from ~1 Hz (e.g., F3 for the 150 to 200 Hz pitch variation) up to ~50 Hz (e.g., F1 for the 250 to 300 Hz pitch variation). For both vowels, the variation in errors across time likely reflects the "fortuitous sampling" effect previously noted in Section IV for baseline linear prediction analysis. Qualitatively, the proposed methods that exploit temporal pitch dynamics reduce the magnitude of this variation in error across time. To quantitatively compare the performance of the tracker using different observation types, we show in Tables IX–X the root mean-squared errors (RMSE) in absolute frequency computed across the full durations of the vowels. The proposed analysis methods provide RMSE reductions ranging from ~2 Hz up to ~25 Hz with respect to the LPCC baseline for the cases considered. In addition, consistent with our observations in Section IV, the relatively poorer performance of the control method suggests that the gains from the projection method are due to its use of temporal pitch dynamics rather than the interpolation method itself. Finally, observe that the overall errors of the LPCC baseline are smaller for the vowel synthesized in the 150 to 200 Hz case relative to the 250 to 300 Hz case. This is consistent with our observations for the traditional linear prediction baseline (Figs. 12–14) showing that errors in formant frequency estimates *increase* with pitch.

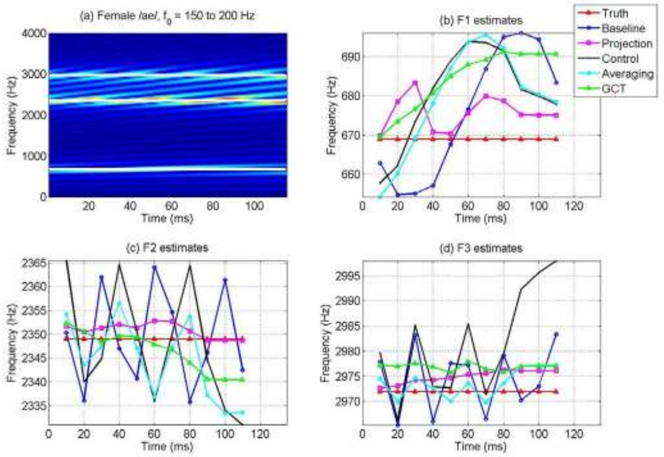

Fig. 19. (a) Spectrogram female vowel /ae/ with pitch 150 to 200 Hz; the spectrogram is computed using a 20-ms Hamming window at a 1-ms frame interval; lines denote true formant frequencies of the vowel. (b) F1 Estimates across time using EKF with different observation types denoted by legend. (c) As in (a) but F2 estimates. (d) As in (a) but F3 esimates.

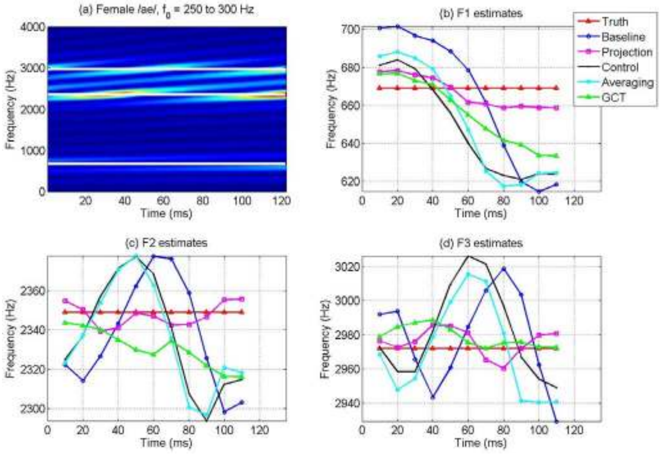

Fig. 20. As in Fig. 19, but for female vowel /ae/ with pitch ranging from 250 to 300 Hz.

TABLE IX
RMSE IN Hz FOR PITCH 150-TO-200-Hz CASE

	F1	F2	F3
LPCC Baseline	17.08	9.8	6.83
Harmonic Projection	7.83	2.32	3.18
Control	16.06	12.03	13.94
Averaging	16.39	9.12	3.19
GCT-based Filtering	16.9	4.89	4.91

TABLE X
RMSE IN Hz FOR PITCH 250-TO-300-Hz CASE

	F1	F2	F3
LPCC Baseline	34.12	29.36	27.36
Harmonic Projection	8.35	5.78	8.48
Control	32.7	29.87	28.15
Averaging	33.85	29	27.16
GCT-based Filtering	21.23	20.66	8.91

Our findings illustrate limitations of standard LPCC analysis for use in the formant tracking task. Observe that absolute errors in formant frequency estimates up to ~50 Hz can result when using LPCCs as observations in a Kalman filtering framework (Figs. 19–20). These effects are due to the inability of LPCCs to accurately represent formant structure under conditions of high pitch from spectral undersampling. Furthermore, our results suggest that by *explicitly* exploiting temporal pitch dynamics in analysis for generating observations, tracking performance can be improved.

VII. Analysis and Tracking of Time-Varying Formants

A limitation of the present work is that it imposes the constraint of a stationary vocal tract throughout analysis. As we have seen in Section IV, this constraint may be reasonable for portions of monophthong vowels; however, this condition is not satisfied for speech sounds where the formant envelope is changing (e.g., diphthongs, glides) as well as transitions from distinct speech sounds (e.g., stop-to-vowel transitions). For the analysis of speech sounds where the formant envelope is changing, the harmonic projection methods (e.g., $m3$ and $m5$) are evidently not directly applicable. A potential extension to these methods could be to project harmonic samples across time *along each formant trajectory*; however, this approach would require *a priori* estimates of the formant trajectories. Alternatively, observe that the GCT can *inherently* maintain source-filter separability when the vocal tract is changing. Specifically, consider a formant transition in a localized region that is increasing in frequency as illustrated in Fig. 21(a). Under this condition, the corresponding $A(\omega, \Omega)$ centered at the origin of the GCT will be rotated at an angle off the Ω-axis as can be shown from standard properties in image processing [14]. Let us denote this direction as a "principle axis," analogous to the Ω-axis when the formant structure is stationary (as in Fig. 8). From the model proposed in Section II, the modulated versions of $A(\omega, \Omega)$ will be located *off* of this principle axis when pitch is either stationary or decreasing (dashed and dotted lines in Fig. 21) [14]. These conditions are analogous to that of increasing and decreasing pitch for the stationary formant case, thereby allowing for improved source-filter separability.

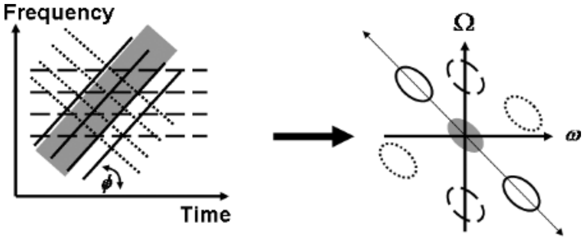

Fig. 21. (a) Localized region of STFT showing a formant transition increasing in frequency (shaded region) along with stationary (dashed), increasing (solid), and decreasing (dotted) pitch harmonics. (b) Corresponding GCT illustrating source-separability of $a[n, m]$ (shaded) from its modulated versions; the double-sided arrow denotes a new "principle axis" analogous to the Ω -axis for a stationary formant. Enhanced separability can be obtained when pitch is either decreasing (dotted) or stationary (dashed).

Conversely, when the pitch harmonics are moving in the same direction as the transition (e.g., increasing, solid lines in Fig. 21), separability can only be obtained when the width of $A(\omega, \Omega)$ along the principle axis is less than the spatial frequency of the 2-D harmonic structure. This is analogous to the condition of *stationary* pitch and formant envelope illustrated in Fig. 8.

To illustrate application to a time-varying formant structure, we show in Fig. 22(a) a pitch-adaptive spectrogram (Sections II, III) computed for a synthetic female diphthong $/\text{ae}/ \rightarrow /\text{iy}/$. The vowel was synthesized using a 135-ms duration source signal as described in Section III with pitch variation from 325 to 275 Hz. A time-varying all-pole (order 6) model with linear formant and bandwidth trajectories was applied to the source signal. The starting and ending formant frequencies of the filter were set to the female monophthongs /ae/ (F1 $=$ 669 Hz, F2 $=$ 2349 Hz, F3 $=$ 2972) and /iy/ (F1 $=$ 437 Hz, F2 $=$ 2761 Hz, F3 $=$ 3372 Hz), respectively. Similarly, the starting and ending bandwidths of the filter were set to the values in Table I for /ae/ and /iy/. In Fig. 22(a), we indicate a local region that contains the third formant transition from 2972 to 3372 Hz (rectangle). Consistent with the model of Fig. 21, the corresponding GCT is shown in Fig. 22(c), and contains components near the origin with orientation off the Ω-axis for some positive value of ϕ. Observe that the modulated versions of this slowly varying envelope are also oriented in this direction (dashed).

To assess the value of analyzing diphthongs using the GCT, we employed GCT-based filtering and the EKF framework (Section IV) for formant estimation of the diphthong shown in Fig. 22(a). For GCT-based analysis, our steps are identical to those described in Section III with the exception of the choice of filter. Specifically, we extracted regions of size 700 Hz by 135 ms (i.e., the full duration of the vowel) with a 350 Hz overlap in frequency. An adaptive 2-D filtering was applied across regions, and overlap-add was used to reconstruct a time–frequency distribution. Observe from Fig. 21 that the 2-D filter for a diphthong would ideally be a low-pass filter along the new "principle axis" corresponding to the orientation of the moving formant structure. This is in contrast to being along the Ω-axis as in the case of monophthongs. In our current development, we approximate this design by using a separable linear-phase low-pass filter as in Section III; however, the filter is designed to capture similar low-frequency content in both

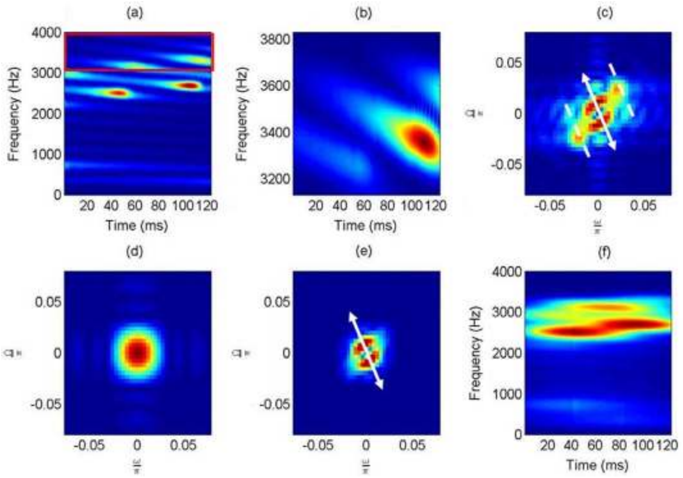

Fig. 22. Filtering in the GCT as in Fig. 11 but for a diphthong. (a) Pitch-adaptive spectrogram and localized region (rectangle) used for computing GCTs. (b) Zoomed-in localized region from (a). (c) $|\mathrm{GCT}_2|$ showing new "principle axis" (solid) corresponding to formant transition and modulated versions with similar orientation (dashed). *For display purposes only, the DC component has been removed*. (d) 2-D circular filter applied to GCT_2. (e) Filtered version of GCT_2 (magnitude) showing "principle axis." (f) Time–frequency reconstruction after filtering.

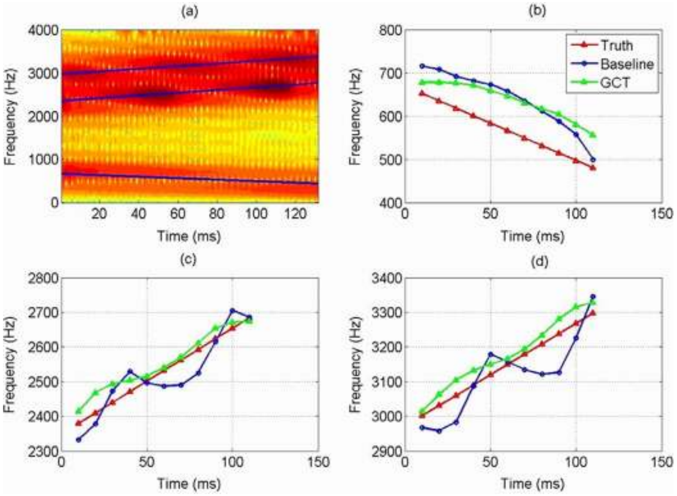

Fig. 23. (a) Broadband log spectrogram of diphthong /ae/ → /iy/ with changing pitch from 325 to 275 Hz; the spectrogram is computed using a 5-ms Hamming window at a 1-ms frame interval; lines denote true formant transitions. (b) F1 estimates obtained from the baseline EKF filter and GCT compared with truth. (c) As in (b) but for F2. (d) As in (b) but for F3.

the ω- and Ω-directions [Fig. 22(d)]. The pass- and stop- bands in *both* the ω and Ω directions were therefore set to $0.25\omega_0$ and ω_0. For the localized region analyzed in Fig. 22(a)–(c), the resulting GCT is shown in Fig. 22(e). Observe that the harmonic components have been removed, and the slowly varying components near the origin are preserved. Fig. 22(f) shows the reconstructed time–frequency distribution from which spectral slices are extracted every 10 ms to generate linear predictive cepstral coefficients (LPCC) as observations to the tracker. This was compared against the baseline 20-ms short-time analysis LPCCs used in Section IV.

Fig. 23 and Table XI show the results of the output of the tracker for both analysis schemes. Fig. 23(a) shows a broadband log-spectrogram of the diphthong with the reference formant frequency trajectories overlain (lines). Observe that due to the high pitch values of the source signal, the formant trajectories do not exhibit smooth transitions across time as may be expected for a low-pitch source. Similar to the observations of Section IV, the baseline tracker exhibits deviations around the true formant frequencies while the GCT-based analysis appears to reduce the magnitude of these deviations [Fig. 23(b)–(d)]. This is quantitatively demonstrated in Table XI, with the GCT-based analysis providing reductions in RMSEs up to ~30 Hz.

TABLE XI
RMSE in Hz of Tracking Results for Female /ae/ to /iy/ With Pitch 150 to 200 Hz

	F1	F2	F3
LPCC Baseline	74.51	45.03	61.99
GCT	72.59	31.1	33

VIII. Conclusion and Future Work

This work has proposed a 2-D processing framework to address formant estimation of high-pitch speakers by exploiting temporal change of pitch. We have shown quantitatively for synthetic signals that our methods outperform traditional and homomorphic linear prediction in formant estimation under conditions of a stationary vocal tract and changing pitch. In addition, we have illustrated the feasibility of the proposed methods for use on natural speech with examples of high-pitch monophthong vowels from female talkers of the TIMIT corpus. We have further demonstrated benefits of the proposed framework in relation to the formant tracking problem in providing improved representations of formant structure under high-pitch conditions for both stationary and time-varying formants. Our results show that the 2-D processing framework is a promising approach for addressing the spectral undersampling problem in formant estimation.

Several future directions are motivated from the current work. The harmonic projection method ($m3$, Section III-B) may be used in conjunction with a method for detecting stationarity of the vocal tract in formant analysis such as in [31]. This may involve incorporating prior information of vowels as proposed by Toda and Tokuda in [32]. Alternatively, an improved filtering method in the GCT domain may be used to better isolate localized formant structure (for both monophthong and diphthong vowels) from its modulated versions. These analysis methods may be used in conjunction with a tracking mechanism towards a full formant estimation system for running speech.

Acknowledgment

The authors would like to thank the reviewers for helpful comments in improving this manuscript. They would also like to thank N. Malyska for use of his software in extracting vowel regions from the TIMIT corpus and D. Rudoy for use of his formant tracking software. Both colleagues also contributed helpful suggestions throughout the course of this work.

References

[1] T. F. Quatieri, "2-D processing of speech with application to pitch estimation," in *Proc. Int. Conf. Spoken Lang. Process.*, Denver, CO, 2002.

[2] T. Ezzat, J. Bouvrie, and T. Poggio, "Spectrotemporal analysis of speech using 2-D Gabor filters," in *Proc. Int. Conf. Spoken Lang. Process.*, Antwerp, Belgium, 2007.

[3] T. Chi, P. W. Ru, and S. A. Shamma, "Multiresolution spectrotemporal analysis of complex sounds," *J. Acoust. Soc. Amer.*, vol. 118, pp. 887–906, 2005.

[4] L. Deng, L. Lee, H. Attias, and A. Acero, "Adaptive Kalman filtering and smoothing for tracking vocal tract resonances using a continuous-valued hidden dynamic model," *IEEE Trans. Audio, Speech, Lang., Process.*, vol. 15, no. 1, pp. 13–23, Jan. 2007.

[5] T. F. Quatieri*, Discrete-Time Speech Signal Processing: Principles and Practice*. Upper Saddle River, NJ: Prentice-Hall, 2001.

[6] A. V. Oppenheim and R. W. Schafer*, Digital Signal Processing*. Englewood Cliffs, NJ: Prentice-Hall, 1975.

[7] S. McAdams, "Segregation of concurrent sounds I: Effects of frequency-modulation coherence," *J. Acoust. Soc. Amer.*, vol. 86, pp. 2148–2159, 1989.

[8] R. L. Diehl, B. Lindblom, K. A. Hoemeke, and R. P. Fahey, "On explaining certain male-female differences in the phonetic realization of vowel categories," *J. Phon.*, pp. 187–208, 1996.

[9] T. T. Wang and T. F. Quatieri, "Exploiting temporal change of pitch in formant estimation," in *Proc. Int. Conf. Acoustics, Speech, Signal Process.*, Las Vegas, NV, 2008, pp. 3929–3932.

[10] T. T. Wang, "Exploiting pitch dynamics for speech spectral estimation using a two-dimensional processing framework," S.M thesis, Dept. Elect. Eng. Comput. Sci., Mass. Inst. of Technol., Cambridge, MA, 2008.

[11] Y. Shiga and S. King, "Estimating the spectral envelope of voiced speech using multi-frame analysis," in *Proc. Eurospeech*, Geneva, Switzerland, 2003.

[12] W. Fisher, G. Doddington, and K. Goudie-Marshall, "The DARPA speech recognition research database: Specifications and status," in *Proc. DARPA Workshop on Speech Recognition*, 1986.

[13] Y. Eldar and A. V. Oppenheim, "Filterbank reconstruction of bandlimited signals from nonuniform and generalized samples," *IEEE Trans. Signal Process.*, vol. 48, no. 10, pp. 2864–2875, Oct. 2000.

[14] R. Gonzalez and R. Woods*, Digital Image Processing*, 2nd ed. Upper Saddle River, NJ: Prentice-Hall, 2002.

[15] D. H. Klatt, "Software for a cascade-parallel formant synthesizer," *J. Acoust. Soc. Amer.*, vol. 67, pp. 971–995, 1980.

[16] J. M. Hillenbrand, L. A. Getty, M. H. Clark, and K. Wheeler, "Acoustic characteristics of American English vowels," *J. Acoust. Soc. Amer.*, vol. 97, pp. 3099–3111, 1995.

[17] H. K. Dunn, "Methods of measuring vowel formant bandwidths," *J. Acoust. Soc. Amer.*, vol. 33, pp. 1737–1746, 1961.

[18] S. Greenberg and H. Hitchcock, "Stress-accent and vowel quality in the switchboard corpus," in *Proc. Workshop on Large-Vocabulary Continuous Speech Recognition*, 2001.

[19] D. Paul, "The spectral envelope estimation vocoder," *IEEE Trans. Acoust., Speech, Signal Process.*, vol. ASSP-29, no. 4, pp. 786–794, Aug. 1981.

[20] F. Fritsch and R. Carlson, "Monotone piecewise cubic interpolation," *SIAM J. Numer. Anal.*, vol. 17, pp. 238–246, 1980.

[21] T. Ezzat, J. Bouvrie, and T. Poggio, "Max-Gabor analysis and synthesis of spectrograms," in *Proc. Int. Conf. Spoken Lang. Process.*, Pittsburgh, PA, 2006.

[22] M. Rahman and T. Shimamura, "Formant frequency estimation of high-pitched speech by homomorphic prediction," *Acoust. Sci. Technol.*, vol. 26, pp. 502–510, 2005.

[23] J. E. Markel and A. H. Gray*, Linear Prediction of Speech*. Secaucus, NJ: Springer-Verlag, 1983.

[24] G. Vallabha and B. Tuller, "Systematic errors in the formant analysis of steady-state vowels," *Speech Commun.*, vol. 38, pp. 141–160, 2002.

[25] P. Boersma, "Praat, a system for doing phonetics by computer," *Glot Int.*, vol. 5, pp. 341–345, 2001.

[26] L. Deng, X. Cui, R. Pruvenok, J. Huang, S. Momen, Y. Chen, and A. Alwan, "A database of vocal tract resonance trajectories for research in speech processing," in *IEEE Int. Conf. Acoust., Speech, Signal Process.*, Toulouse, France, 2006, pp. I-369–I-372.

[27] M. Plumpe, T. F. Quatieri, and D. Reynolds, "Modeling of the glottal flow derivative waveform with application to speaker identification," *IEEE Trans. Speech Audio Process.*, vol. 7, no. 5, pp. 569–586, Sep. 1999.

[28] A. E. Rosenberg, "Effect of the glottal pulse shape on the quality of natural vowels," *J. Acoust. Soc. Amer.*, vol. 49, pp. 583–590, 1971.

[29] K. N. Stevens*, Acoustic Phonetics*. Cambridge, MA: MIT Press, 1998.

[30] D. Rudoy, D. Spendley, and P. J. Wolfe, "Conditionally linear gaussian models for tracking vocal tract resonances," in *Proc. Interspeech*, Antwerp, Belgium, 2007.

[31] P. Basu, D. Rudoy, and P. J. Wolfe, "A nonparametric test for stationarity based on local Fourier analysis," in *IEEE Int. Conf. Acoust., Speech, Signal Process.*, Taipei, Taiwan, 2009, pp. 3005–3008.

[32] T. Toda and K. Tokuda, "Statistical approach to vocal tract transfer function estimation based on factor analyzed trajectory HMM," in *IEEE Int. Conf. Acoustics Speech and Signal Processing*, Las Vegas, NV, 2008, pp. 3925–3928.

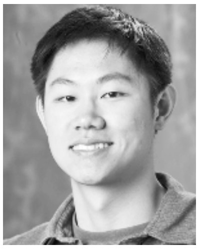

Tianyu T. Wang (S'02) received the B.S. degree (with highest honors) in electrical engineering from the Georgia Institute of Technology, Atlanta, in 2005 and the S.M. degree in electrical engineering from the Massachusetts Institute of Technology (MIT), Cambridge, MA, in 2008. He is currently pursuing the Ph.D. degree at the Harvard-MIT Division of Health Sciences and Technology, Cambridge.

He was a National Science Foundation summer intern with the Landmark-Based Speech Recognition Group at the Center for Language and Speech Processing's (Johns Hopkins University) Summer Research Workshop in 2004, where he worked on acoustic phonetic feature extraction and classification. He is currently a Graduate Research Assistant at MIT Lincoln Laboratory, Lexington, where, in the S.M. program, he worked on formant estimation methods motivated from auditory modeling. His research interests are in signal processing, detection/estimation theory, and auditory modeling with application to speech separation, enhancement, and recognition.

Mr. Wang is a member of Eta Kappa Nu.

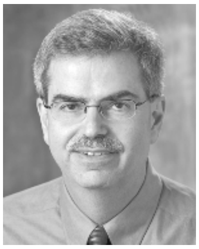

Thomas F. Quatieri (S'73–M'79–SM'87–F'98) received the B.S. degree (*summa cum laude*) from Tufts University, Medford, MA, in 1973, and the S.M., E.E., and Sc.D. degrees from the Massachusetts Institute of Technology (MIT), Cambridge, in 1975, 1977, and 1979, respectively.

He is currently a Senior Member of the Technical Staff with MIT Lincoln Laboratory, Lexington, involved in digital signal processing for speech and audio applications and in nonlinear signal processing. He also holds the position of faculty in the MIT Speech and Hearing Bioscience and Technology Program which is under the Harvard-MIT Division of Health Sciences and Technology. His current interests include speech enhancement, modification, and encoding algorithms inspired by nonlinear biological models of speech production and auditory processing, and automatic and human speaker and dialect recognition. He is the author of the textbook *Discrete-Time Speech Signal Processing: Principles and Practice* (Prentice-Hall, 2001) and has developed the MIT graduate course Digital Speech Processing. He is also active in advising graduate students on the MIT campus.

Dr. Quatieri is the recipient of the 1982 Paper Award of the IEEE Signal Processing Society, both the 1990 and 1994 IEEE Signal Processing Society's Senior Award, and the 1995 IEEE W. R. G. Baker Prize Award. He has been a member of the IEEE Digital Signal Processing Technical Committee, from 1983 to 1992 was a member of the steering committee of the biannual Digital Signal Processing Workshop, and has served on the IEEE Speech Technical Committee. He has also served as Associate Editor for the IEEE TRANSACTIONS ON SIGNAL PROCESSING in the area of nonlinear systems and is currently on the IEEE James L. Flanagan Speech and Audio Awards committee. Dr. Quatieri is a member of Tau Beta Pi, Eta Kappa Nu, Sigma Xi, and the Acoustics Society of America.